International Journal of Fracture **76:** 243–261, 1996.

Analysis of newly-defined stress intensity factors for angular corners using singular integral equations of the body force method

N.-A. NODA[1], K. ODA[2] and T. INOUE[1]
[1]*Department of Mechanical Engineering, Kyushu Institute of Technology, 1-1 Sensui-cho, Tobata, Kitakyushu 804, Japan*
[2]*Department of Mechanical and Electrical Engineering, Tokuyama College of Technology, 3538 Takajo, Kume, Tokuyama 745, Japan*

Received 20 April 1995; accepted in revised form 18 October 1995

Abstract. In this study, numerical solutions of singular integral equations are discussed in the analysis of angular corners. The problems are formulated as a system of singular integral equations on the basis of the body force method. In the numerical solutions, two types of fundamental density functions are chosen to express the symmetric type stress singularity of $1/r^{1-\lambda_1}$ and the skew-symmetric type stress singularity of $1/r^{1-\lambda_2}$; then the unknown functions are expressed as a linear combination of the fundamental density functions and power series. The calculation shows that the present method gives rapidly converging numerical results for angular corners as well as ordinary cracks in homogeneous materials. The stress intensity factors of angular corners are calculated for various geometrical and loading conditions.

1. Introduction

In recent decades, the use of composite materials increased in a wide range of engineering fields and the accurate evaluation of interface strength in dissimilar materials has become very important. The fracture of composites and dissimilar materials is commonly observed at an interface because the angular corner of bonded materials induces singular stress and crack initiation at the interface. Hence, problems of angular corners in dissimilar materials have been treated in many papers [1–8]. Recently, Chen and Nisitani pointed out that in this problem there appear to be two types of stress singularities $1/r^{1-\lambda_1}$ and $1/r^{1-\lambda_2}$, where $1-\lambda_1$ and $1-\lambda_2$ are the orders of singularity of the stress field for the mode I deformation and mode II deformation, respectively [9–11]. Then, it is necessary that both intensities of the singular stress field corresponding to mode I and mode II are evaluated exactly.

In our previous papers, the numerical solutions of the singular integral equation of the body force method in crack problems have been discussed [12–15]. Then, the numerical method, in which unknown functions are approximated by the products of fundamental density functions and polynomials, has been found to give results of high accuracy with short CPU time. In this paper, the method is applied to the problems of notch or holes with angular corners and the extended stress intensity factors of these problems are obtained. The present problems are regarded as a fundamental problem of composite materials because the stress singularity at the bonded corner of the composite materials is essentially the same as the problem of the angular corner in an homogeneous plate. In the numerical solution, two types of fundamental density functions are used to express two types of stress singularities. The accurate stress intensity factors of the angular corners are calculated for various geometrical and loading conditions and interaction effect of angular corners is also discussed in comparison with the problem of ordinary cracks.

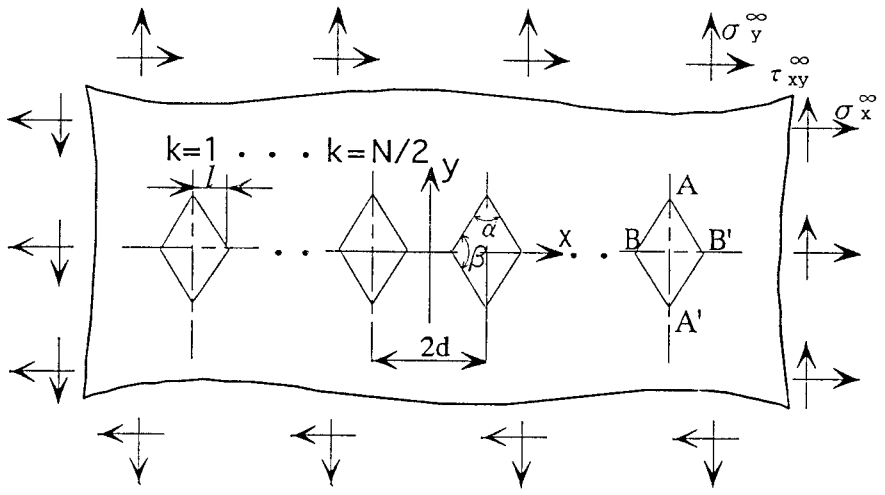

Figure 1. Diamond-shaped holes in an infinite plate. (When the number of holes is an even number.)

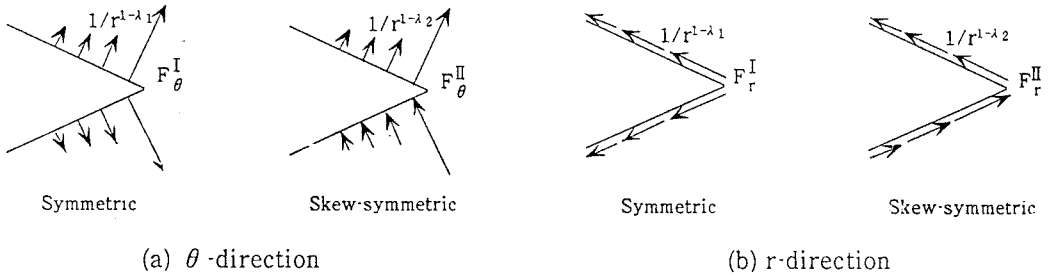

Figure 2. Two types of pairs of body forces distributed along the imaginary boundary with angular corner.

2. Numerical solution of angular corners

According to Chen's study, the singular stress field at an angular corner due to in-plane deformation is expressed as a sum of the symmetric state with stress singularity $1/r^{1-\lambda_1}$ and the skew-symmetric state with stress singularity $1/r^{1-\lambda_2}$ [9–11].

$$\sigma_{ij} = \frac{K_{\mathrm{I},\lambda_1}}{r^{1-\lambda_1}} f_{ij}^{\mathrm{I}}(\theta) + \frac{K_{\mathrm{II},\lambda_2}}{r^{1-\lambda_2}} f_{ij}^{\mathrm{II}}(\theta). \tag{1}$$

In (1) the singular stress field near an angular corner is defined in terms of two parameters, K_{I,λ_1} and $K_{\mathrm{II},\lambda_2}$, which express the intensities of the singular stress field in a similar way to the stress intensity factor in ordinary cracks.

Consider any number of diamond-shaped holes with the same size in an infinite plate as a fundamental problem to explain the solution of an angular corner (Figure 1). In this analysis, two types of pairs of body forces, that is, a symmetric type (mode I) and a skew-symmetric type (mode II) to the bisector of the corner A, are distributed along the imaginary boundary in an infinite plate without the holes as shown in Figure 2. These body forces are also distributed around the corners A', B, B' and imaginary boundaries of the other diamond

holes in a similar manner. Since the orders of stress singularity are different between the corners A and B, the side of the diamond-shaped hole is divided into two equal parts for the convenience of numerical analysis. Based on the body force method mentioned above, the integral equations, which are virtually the boundary conditions ($\sigma_n = 0$ and $\tau_{nt} = 0$) on the imaginary boundary of the ith diamond-shaped hole containing the corner A, are expressed as follows, where the body force densities distributed in the θ- and r-directions, $F_{\theta,k} = F^{\mathrm{I}}_{\theta,k} + F^{\mathrm{II}}_{\theta,k}$ and $F_{r,k} = F^{\mathrm{I}}_{r,k} + F^{\mathrm{II}}_{r,k}$, are unknown functions.

$$
\begin{aligned}
-\tfrac{1}{2}F_{\theta A,i}(s_i) + \sum_{k=1}^{N/2}\Bigg[& \int_0^{l_{AB}/2} h_{nn}^{F_{\theta,k}}(r_{A,k}, s_i)F_{\theta A,k}(r_{A,k})\,\mathrm{d}r_{A,k} \\
& + \int_0^{l_{AB}/2} h_{nn}^{F_{r,k}}(r_{A,k}, s_i)F_{rA,k}(r_{A,k})\,\mathrm{d}r_{A,k} \\
& + \int_0^{l_{AB}/2} h_{nn}^{F_{\theta,k}}(r_{A',k}, s_i)F_{\theta A',k}(r_{A',k})\,\mathrm{d}r_{A',k} \\
& + \int_0^{l_{AB}/2} h_{nn}^{F_{r,k}}(r_{A',k}, s_i)F_{rA',k}(r_{A',k})\,\mathrm{d}r_{A',k} \\
& + \int_0^{l_{AB}/2} h_{nn}^{F_{\theta,k}}(r_{B,k}, s_i)F_{\theta B,k}(r_{B,k})\,\mathrm{d}r_{B,k} \\
& + \int_0^{l_{AB}/2} h_{nn}^{F_{r,k}}(r_{B,k}, s_i)F_{rB,k}(r_{B,k})\,\mathrm{d}r_{B,k} \\
& + \int_0^{l_{AB}/2} h_{nn}^{F_{\theta,k}}(r_{B',k}, s_i)F_{\theta B',k}(r_{B',k})\,\mathrm{d}r_{B',k} \\
& + \int_0^{l_{AB}/2} h_{nn}^{F_{r,k}}(r_{B',k}, s_i)F_{rB',k}(r_{B',k})\,\mathrm{d}r_{B',k}\Bigg] = -\sigma_n^{\infty}(s_i)
\end{aligned}
$$

$$
\begin{aligned}
-\tfrac{1}{2}F_{rA,i}(s_i) + \sum_{k=1}^{N/2}\Bigg[& \int_0^{l_{AB}/2} h_{nt}^{F_{\theta,k}}(r_{A,k}, s_i)F_{\theta A,k}(r_{A,k})\,\mathrm{d}r_{A,k} \\
& + \int_0^{l_{AB}/2} h_{nt}^{F_{r,k}}(r_{A,k}, s_i)F_{rA,k}(r_{A,k})\,\mathrm{d}r_{A,k} \\
& + \int_0^{l_{AB}/2} h_{nt}^{F_{\theta,k}}(r_{A',k}, s_i)F_{\theta A',k}(r_{A',k})\,\mathrm{d}r_{A',k} \\
& + \int_0^{l_{AB}/2} h_{nt}^{F_{r,k}}(r_{A',k}, s_i)F_{rA',k}(r_{A',k})\,\mathrm{d}r_{A',k}
\end{aligned}
$$

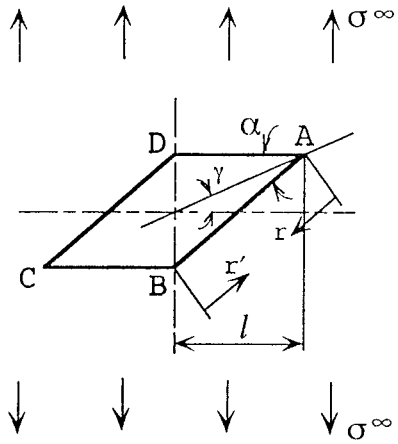

Figure 3. Parallelogram hole in an infinite plate.

$$+\int_0^{l_{AB}/2} h_{nt}^{F_{\theta,k}}(r_{B,k}, s_i) F_{\theta B,k}(r_{B,k})\,\mathrm{d}r_{B,k}$$

$$+\int_0^{l_{AB}/2} h_{nt}^{F_{r,k}}(r_{B,k}, s_i) F_{rB,k}(r_{B,k})\,\mathrm{d}r_{B,k}$$

$$+\int_0^{l_{AB}/2} h_{nt}^{F_{\theta,k}}(r_{B',k}, s_i) F_{\theta B',k}(r_{B',k})\,\mathrm{d}r_{B',k}$$

$$+\int_0^{l_{AB}/2} h_{nt}^{F_{r,k}}(r_{B',k}, s_i) F_{rB',k}(r_{B',k})\,\mathrm{d}r_{B',k}\Big] = -\tau_{nt}^{\infty}(s_i)$$

$$i = 1 \sim N/2. \tag{2}$$

In (2) the first term represents the stress due to the body force distributed on $\ominus$ boundary. The $\ominus$ boundary means the imaginary boundary composed of the internal points that are infinitesimally apart from the initial boundary [17, 18]. Taking $h_{nn}^{F_{\theta,k}}(r_{A,k}, s_i)$ for example, the notation means the normal stress σ_n induced at the collocation point s_i on the imaginary boundary of the ith diamond-shaped hole when the body force with unit density in the θ-direction is acting at the point $r_{A,k}$ on the imaginary boundary of the kth diamond-shaped hole, where s_i and $r_{A,k}$ are distances measured from the corner A. The body forces are symmetrically or skew-symmetrically distributed with respect to the y-axis. The notations $\sigma_n^{\infty}(s_i)$ and $\tau_{nt}^{\infty}(s_i)$ in (2) are normal and shear stresses at the point s_i in an infinite plate without the diamond holes. The boundary integral equations corresponding to other corners are also expressed in a similar way.

In this study, the unknown functions of the body force densities, $F_{\theta A,k}$ and $F_{rA,k}$, are approximated by a linear combination of power series and two types of fundamental density functions.

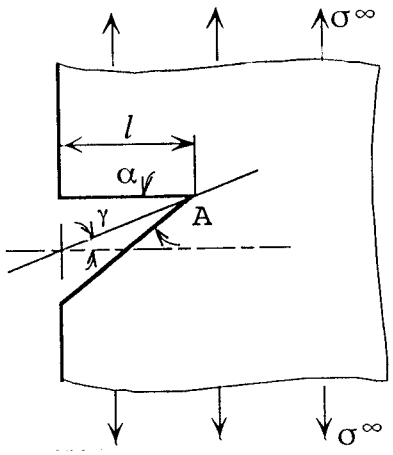

Figure 4. V-shaped notch in a semi-infinite plate.

$$\begin{aligned} F_{\theta A,k}(r_{A,k}) &= F^{\mathrm{I}}_{\theta A,k}(r_{A,k}) + F^{\mathrm{II}}_{\theta A,k}(r_{A,k}) \\ &= W^{\mathrm{I}}_{\theta A,k}(r_{A,k}) r_{A,k}^{\lambda_1-1} + W^{\mathrm{II}}_{\theta A,k}(r_{A,k}) r_{A,k}^{\lambda_2-1} \\ F_{rA,k}(r_{A,k}) &= F^{\mathrm{I}}_{rA,k}(r_{A,k}) + F^{\mathrm{II}}_{rA,k}(r_{A,k}) \\ &= W^{\mathrm{I}}_{rA,k}(r_{A,k}) r_{A,k}^{\lambda_1-1} + W^{\mathrm{II}}_{rA,k}(r_{A,k}) r_{A,k}^{\lambda_2-1} \end{aligned} \tag{3}$$

$$W^{\mathrm{I}}_{\theta A,k}(r_{A,k}) = \sum_{n=1}^{M} a_{n,k} r_{A,k}^{n-1}, \qquad W^{\mathrm{II}}_{\theta A,k}(r_{A,k}) = \sum_{n=1}^{M} b_{n,k} r_{A,k}^{n-1},$$

$$W^{\mathrm{I}}_{rA,k}(r_{A,k}) = \sum_{n=1}^{M} c_{n,k} r_{A,k}^{n-1}, \qquad W^{\mathrm{II}}_{rA,k}(r_{A,k}) = \sum_{n=1}^{M} d_{n,k} r_{A,k}^{n-1}. \tag{4}$$

Here, $r_{A,k}^{\lambda_1-1}$ and $r_{A,k}^{\lambda_2-1}$ are the fundamental density functions to express the stress singularities of mode I and mode II at the angular corner A on the imaginary boundary of the kth diamond hole, respectively [10]. The superscripts I and II mean the distribution types of body force, that is, symmetrical (mode I) and skew-symmetrical (mode II) to the bisector of the corner, respectively. In the case of the sharp notch with vertex angle α, the eigenvalues λ_1 and λ_2 are given as the roots of the following eigenequations [10]

$$\begin{aligned} &\text{mode I}: \quad \sin[\lambda_1(2\pi - \alpha)] = \lambda_1 \sin\alpha, \\ &\text{mode II}: \quad \sin[\lambda_2(2\pi - \alpha)] = -\lambda_2 \sin\alpha. \end{aligned} \tag{5}$$

By using the numerical method mentioned above, the integral equations are solved and the unknown coefficients $a_{n,k}, b_{n,k}, c_{n,k}$ and $d_{n,k}$ are determined. The stress intensity factors $K_{\mathrm{I},\lambda_1,k}, K_{\mathrm{II},\lambda_2,k}$ of the angular corner A of the kth diamond-shaped holes defined by (1) can be obtained from the values of $W^{\mathrm{I}}_{\theta A,k}(0), W^{\mathrm{II}}_{\theta A,k}(0), W^{\mathrm{I}}_{rA,k}(0)$ and $W^{\mathrm{II}}_{rA,k}(0)$ at the corner tip A [10].

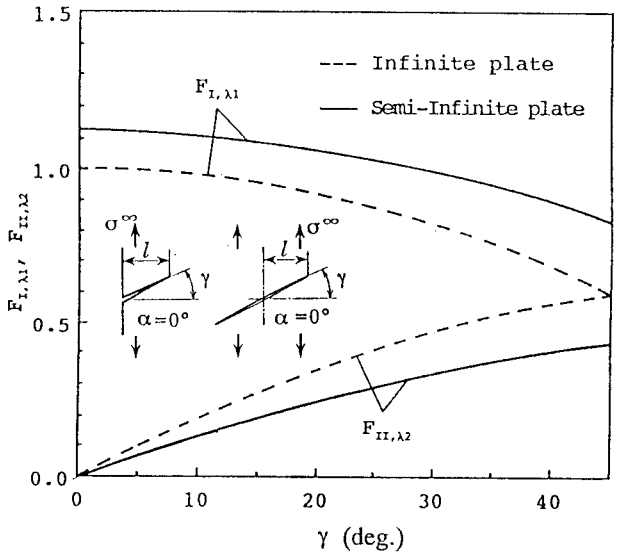

Figure 5a.

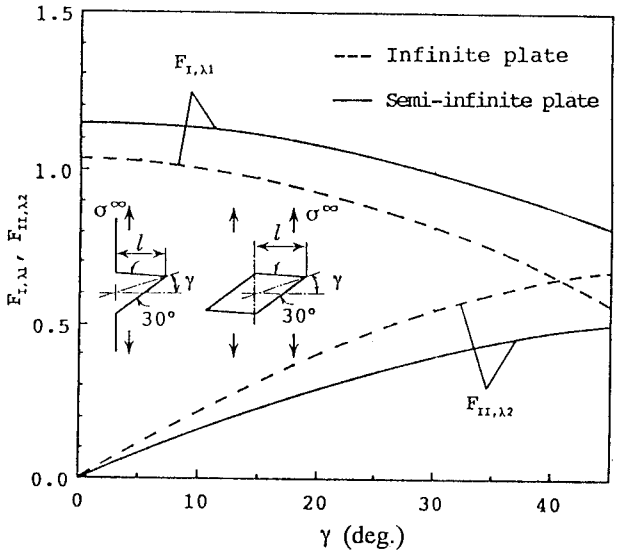

Figure 5b.

3. Results and discussion

3.1. Sharp notch problems in an infinite plate and in a semi-infinite plate

As fundamental problems of an angular corner, a parallelogram hole in an infinite plate and a V-shaped notch in a semi-infinite plate are analyzed (see Figures 3 and 4). The stress intensity factors of angular corner, K_{I,λ_1} and K_{II,λ_2}, obtained by the present analysis are written by the following dimensionless expressions

$$F_{I,\lambda_1} = \frac{K_{I,\lambda_1}}{\sigma^{\infty}\sqrt{\pi}l^{1-\lambda_1}}, \qquad F_{II,\lambda_2} = \frac{K_{II,\lambda_2}}{\sigma^{\infty}\sqrt{\pi}l^{1-\lambda_2}}. \tag{6}$$

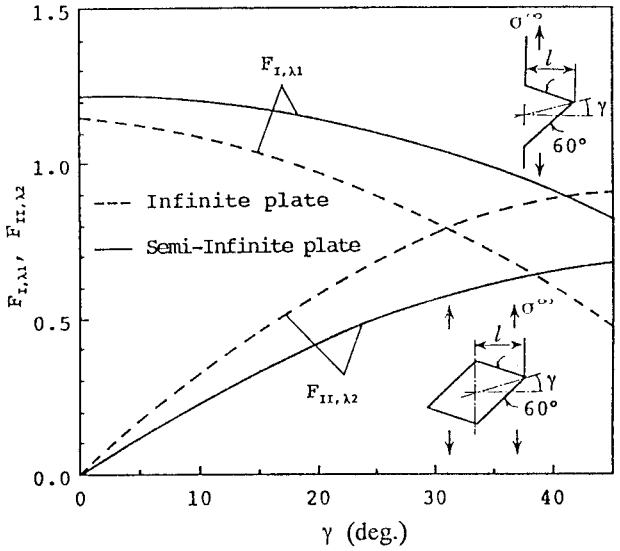

Figure 5. $F_{I,\lambda_1}, F_{II,\lambda_2} - \gamma$ relations. (a) $\alpha = 0°(\lambda_1 = 0.5, \lambda_2 = 0.5)$, (b) $\alpha = 30°(\lambda_1 = 0.5014530, \lambda_2 = 0.5981918)$, (c) $\alpha = 60°(\lambda_1 = 0.5122214, \lambda_2 = 0.7309007)$.

Table 1. Convergency of the present result of V-shaped notch ($\alpha = 60°, \beta = 30°$ in Figure 4)

M	F_{I,λ_1} $\lambda_1 = 0.5122214$		F_{II,λ_2} $\lambda_2 = 0.7309007$	
	from $W_\theta^I(0)$	from $W_r^I(0)$	from $W_\theta^{II}(0)$	from $W_r^{II}(0)$
2	0.90412	0.84967	0.59667	0.61162
4	1.07587	1.09915	0.58194	0.57702
6	1.04600	1.05007	0.58066	0.58012
8	1.04263	1.04419	0.57668	0.57679
10	1.04177	1.04252	0.57691	0.57675
12	1.04132	1.04182	0.57699	0.57688
14	1.04114	1.04148	0.57687	0.57681
16	1.04099	1.04123	0.57688	0.57683
18	1.04093	1.04111	0.57685	0.57681
20	1.04085	1.04100	0.57684	0.57682
22	1.04083	1.04094	0.57684	0.57682
Chen [2]	1.040*		0.577*	

* Extrapolated value from the results of $M = 40$ and 100.

First, the accuracy of the present method for these problems is examined. The values of K_{I,λ_1} and K_{II,λ_2} can be determined from the values of $W_\theta^I(0)$ and $W_\theta^{II}(0)$ at the corner tip, respectively [10]. By using the values of $W_r^I(0)$ and $W_r^{II}(0)$, K_{I,λ_1} and K_{II,λ_2} can also be determined. Both values of K_{I,λ_1} (or K_{II,λ_2}) obtained from values of weight functions in θ- and r-direction at the corner tip should be in agreement with each other within the error of numerical calculation. Taking the problem of the V-shaped notch in a semi-infinite plate ($\alpha = 60°, \gamma = 30°$ in Figure 4) as an example, the convergency of the F_{I,λ_1} and F_{II,λ_2} with increasing the number of collocation points M is shown in Table 1. For reference, Chen's

Table 2. Compliance with the boundary condition near the angular corner (r: Distance from corner tip A in Figure 4)

$\alpha = 60°, \gamma = 30°, M = 20$		
r/l_{AB}	σ_n	τ_{nt}
0.01	$-2.8699E$-04	$1.2971E$-04
0.02	$1.0475E$-04	$-1.6635E$-04
0.03	$2.0660E$-05	$-1.4201E$-04
0.04	$2.3489E$-06	$3.3265E$-05
0.05	$3.9110E$-05	$1.3906E$-04
0.06	$5.2104E$-05	$1.2401E$-04
0.07	$1.9843E$-05	$3.6819E$-05
0.08	$-3.3566E$-05	$-5.4891E$-05
0.09	$-7.3811E$-05	$-1.0562E$-04
0.10	$-7.9306E$-05	$-1.0286E$-04

results are also shown in Table 1. Chen and Nisitani [10] have analyzed the problem using the body force method, in which the unknown functions have been approximated by the piecewise linear function with the fundamental density functions at each divided interval. Chen's results are the extrapolated value from the results of $M = 40$ and 100 on the basis of the linear relationship between the SIF and $1/M$. The present results have good convergency and the results obtained from values of weight function in θ- and r-direction coincide with each other in about four digits when $M = 14$. Table 2 shows the compliance with the boundary condition ($\sigma_n = 0$ and $\tau_{nt} = 0$) near the angular corner. The values of σ_n and τ_{nt} which should be zero along the notch boundary are less than 10^{-4} even when $M = 20$. Therefore it is confirmed that the present numerical method is useful for analyzing this problem.

Table 3 shows F_{I,λ_1} and $F_{\mathrm{II},\lambda_2}$ at the corner A when the values of α and γ are changed systematically in the problems illustrated in Figures 3 and 4. The results of the V-shaped notch in a semi-infinite plate are shown in comparison with the result obtained by Chen and Nisitani [10]. From Table 3, both results are found to be in good agreement. In Figure 5(a)–(c), $F_{\mathrm{I},\lambda_1} - \gamma$ and $F_{\mathrm{II},\lambda_2} - \gamma$ relations are shown. The values for an infinite plate are shown by the dashed lines in Figure 5. It is found that the values of F_{I,λ_1} for a semi-infinite plate are always larger than that for an infinite plate in all the ranges of $0° \leqslant \gamma \leqslant 45°$. On the other hand, the values of $F_{\mathrm{II},\lambda_2}$ for a semi-infinite plate are always smaller than those for an infinite plate. The tendency to variation of dimensionless SIFs of the angular corner ($\alpha = 30°$ and 60°) by increasing the angle β is similar to that of crack problem ($\alpha = 0°$).

3.2. Interaction problem of diamond-shaped holes

The interaction problem of two and any number of diamond-shaped holes with the same shape and size under various loading conditions is analyzed (see Figure 1). Table 4 shows the convergency of the F_{I,λ_1} and $F_{\mathrm{II},\lambda_2}$ at the corner A by increasing the collocation number M when the number of diamond-shaped holes $N = 2, \alpha = 30°, \lambda = l/d = \frac{1}{2}$ and $\sigma_x^\infty = \sigma_y^\infty = \sigma^\infty, \tau_{xy}^\infty = 0$ as in Figure 1. The present results have good convergency and the results obtained from values of weight functions in θ- and r-direction coincide with each other in

Table 3. Dimensionless SIFs F_{I,λ_1} and $F_{\mathrm{II},\lambda_2}$ for a parallelogram hole (Figure 3) and a V-shaped notch (Figure 4)

α	γ	Infinite plate (Figure 3)		Semi-infinite plate (Figure 4)			
				Present analysis		Chen-Nisitani [2]	
		F_{I,λ_1}	$F_{\mathrm{II},\lambda_2}$	F_{I,λ_1}	$F_{\mathrm{II},\lambda_2}$	F_{I,λ_1}	$F_{\mathrm{II},\lambda_2}$
	0°	1.000	0.000	1.122	0.000	1.122	0.000
	5°	0.994	0.087	1.118	0.060	1.118	0.060
0°	15°	0.949	0.254	1.088	0.177	1.088	0.177
	30°	0.806	0.465	0.989	0.329	0.989	0.329
	45°	0.595	0.595	0.838	0.433	0.838	0.433
	0°	1.011	0.000	1.129	0.000		
	5°	1.004	0.093	1.125	0.066		
15°	15°	0.957	0.271	1.094	0.194		
	30°	0.809	0.492	0.991	0.358		
	45°	0.594	0.619	0.829	0.467		
	0°	1.042	0.000	1.147	0.000	1.148	0.000
	5°	1.032	0.108	1.145	0.075	1.140	0.075
30°	15°	0.977	0.308	1.111	0.218	1.107	0.218
	30°	0.816	0.551	1.003	0.398	1.000	0.397
	45°	0.575	0.681	0.834	0.507	0.834	0.505
	0°	1.088	0.000	1.182	0.000		
	5°	1.073	0.132	1.177	0.089		
45°	15°	1.006	0.367	1.139	0.258		
	30°	0.811	0.646	1.021	0.464		
	45°	0.513	0.768	0.834	0.574		
	0°	1.148	0.000	1.225	0.000	1.225	0.000
	5°	1.125	0.170	1.220	0.113	1.218	0.113
60°	15°	1.040	0.463	1.178	0.327	1.176	0.326
	30°	0.805	0.789	1.041	0.577	1.040	0.577
	45°	0.485	0.905	0.825	0.685	0.824	0.684
	0°	1.217	0.000	1.277	0.000		
	5°	1.187	0.243	1.271	0.163		
75°	15°	1.084	0.646	1.221	0.469		
	30°	0.817	1.074	1.059	0.809		
	45°	0.416	1.158	0.795	0.902		
	0°	1.293	0.000	1.336	0.000	1.336	0.000
	5°	1.258	0.471	1.328	0.331	1.327	0.331
90°	15°	1.139	1.244	1.267	0.946	1.266	0.946
	30°	0.823	2.077	1.066	1.575	1.065	1.576

about five digits when $M = 18$. Therefore the present numerical method is also useful for the interaction problem.

Table 5 shows F_{I,λ_1} and $F_{\mathrm{II},\lambda_2}$ at the corner A ($\alpha \leqslant 90°$) when $N = 2$ and the values of $\lambda = l/d$ and α are changed systematically. Here, three kinds of fundamental loads at infinity,

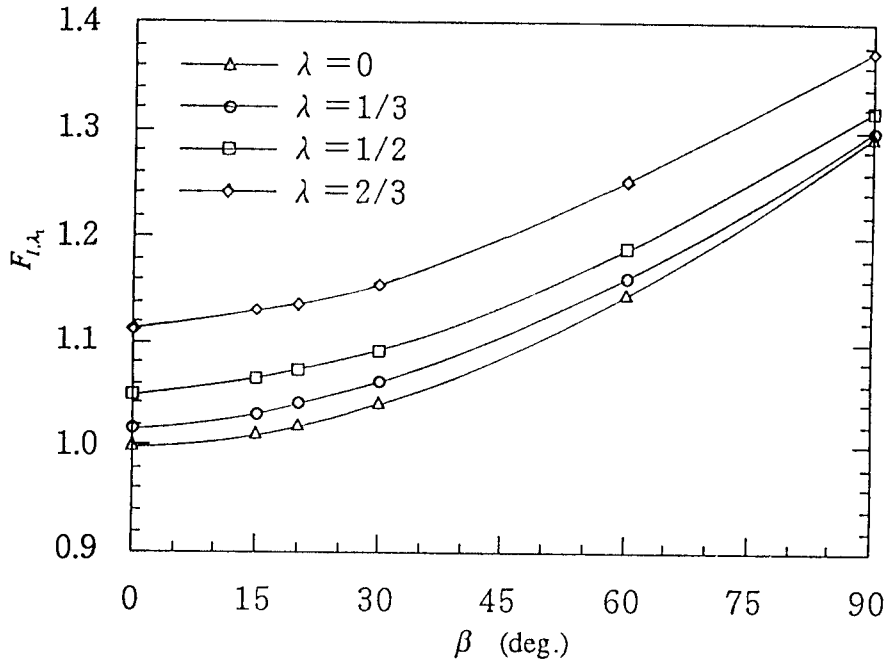

Figure 6. An example of $F_{\mathrm{II},\lambda_2} - \beta$ relation. ($\tau_{xy}^{\infty} = \tau^{\infty}, \sigma_x^{\infty} = \sigma_y^{\infty} = 0$).

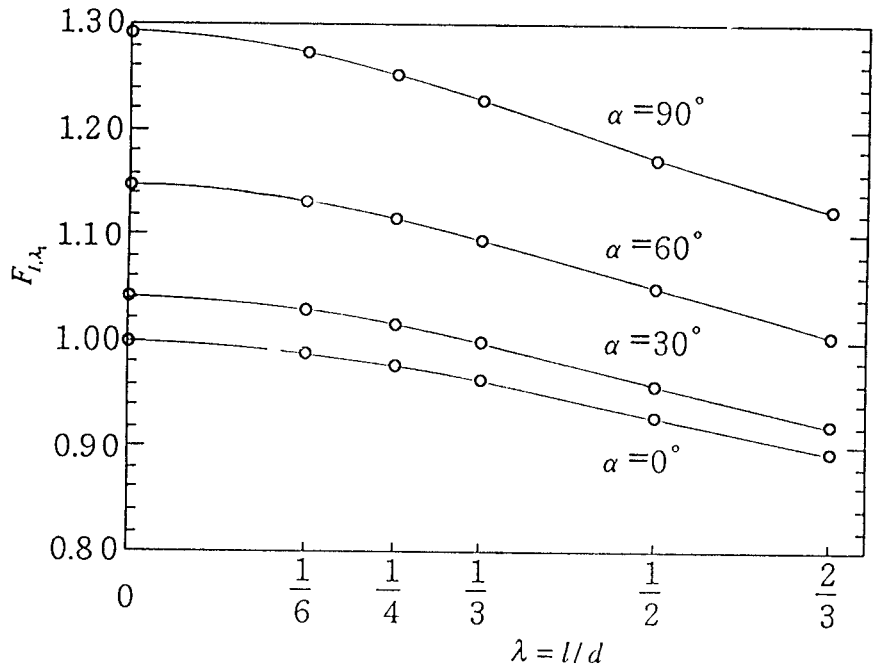

Figure 7. An example of $F_{\mathrm{I},\lambda_1} - \lambda$ relation. ($\sigma_x^{\infty} = \sigma^{\infty}, \sigma_y^{\infty} = \tau_{xy}^{\infty} = 0$).

Table 4. Convergency of F_{I,λ_1} and $F_{\mathrm{II},\lambda_2}$ for two diamond-shaped holes. ($N = 2, \alpha = 30°, \lambda = l/d = \frac{1}{2}, \sigma_x^\infty = \sigma_y^\infty = \sigma^\infty, \tau_{xy}^\infty = 0$ in Figure 1)

M	$F_{\mathrm{I},\lambda_1}(\lambda_1 = 0.5014530)$		$F_{\mathrm{II},\lambda_2}(\lambda_2 = 0.5981918)$	
	from $W_r^{\mathrm{I}}(0)$	from $W_\theta^{\mathrm{I}}(0)$	from $W_r^{\mathrm{II}}(0)$	from $W_\theta^{\mathrm{II}}(0)$
2	0.98816	0.99747	0.26062	0.25870
4	0.94644	0.94663	0.02273	0.02271
6	0.94476	0.94473	0.02257	0.02257
8	0.94433	0.94431	0.02252	0.02252
10	0.94414	0.94413	0.02250	0.02250
12	0.94405	0.94404	0.02249	0.02494
14	0.94399	0.94398	0.02249	0.02249
16	0.94396	0.94395	0.02249	0.02248
18	0.94394	0.94394	0.02248	0.02248

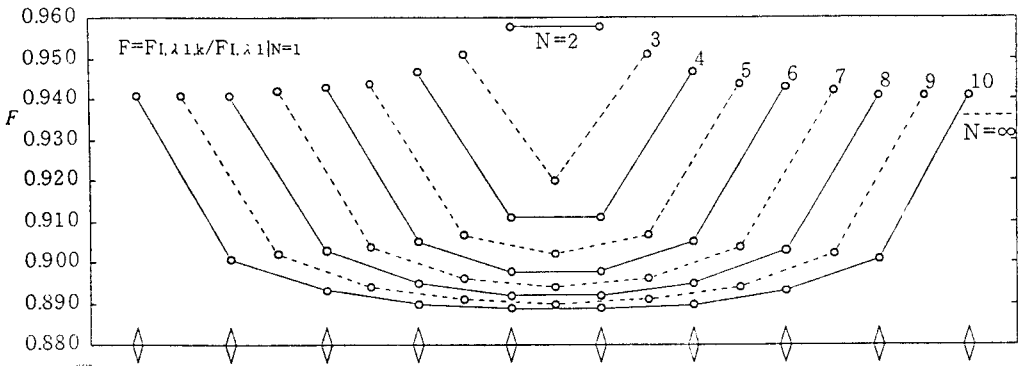

Figure 8. F for each diamond-shaped hole at the corner A. ($\sigma_x^\infty = \sigma^\infty, \sigma_y^\infty = \tau_{xy}^\infty = 0$, $\alpha = 30°$, $\lambda = \frac{1}{3}$).

that is, uniaxial tension, biaxial tension and in-plane shear are treated. The values of $\alpha = 0°$ are the results for the way that the body force densities are approximated by Chebyshev polynomials and two types of fundamental density functions [13]. In Table 6, F_{I,λ_1} and $F_{\mathrm{II},\lambda_2}$ at the corners B and B' ($\beta \leqslant 90°$) under three types of loads are shown. The values of $\beta = 0°$ are the exact solution for the two collinear cracks with the same length given by Erdogan [15]. From the values of Tables 5 and 6, Figure 6 shows $F_{\mathrm{I},\lambda_1} - \beta$ relations at the corners B and B' when $\sigma_y^\infty = \sigma^\infty, \sigma_x^\infty = \tau_{xy}^\infty = 0$ and Figure 7 shows $F_{\mathrm{I},\lambda_1} - \lambda$ relations at the corner A when $\sigma_x^\infty = \sigma^\infty, \sigma_y^\infty = \tau_{xy}^\infty = 0$. From Figure 6, as $\beta \to 0°$, the values of the stress intensity factors ($F_{\mathrm{I},\lambda_1}, F_{\mathrm{II},\lambda_2}$) decrease and coincide with the exact solution for the two collinear cracks. On the other hand, from Figure 7, as $\lambda \to 0$, these values coincide with the results of single diamond-shaped holes.

Figures 8 and 9 show the values of the stress intensity factors ($F_{\mathrm{I},\lambda_1,k}$ and $F_{\mathrm{II},\lambda_2,k}$) at the corner A of each diamond-shaped hole when $N = 2 \sim 10, \alpha = 30°, \lambda = l/d = \frac{1}{3}$ for uniaxial tension and in-plane shear. Figures 10 and 11 show the values of the stress intensity factors ($F_{\mathrm{I},\lambda_1,k}$) at the corners B and B' of each diamond-shaped hole when $N = 2 \sim 10, \beta = 30°, \lambda = l/d = \frac{1}{3}$ for uniaxial tension (y-direction) and biaxial tension. The vertical axis of these figures indicates the ratio of $F_{\mathrm{I},\lambda_1,k}$ (or $F_{\mathrm{II},\lambda_2,k}$) to $F_{\mathrm{I},\lambda_1}|_{N=1}$ (or $F_{\mathrm{II},\lambda_2}|_{N=1}$). In Figure 8,

Table 5. F_{I,λ_1} and $F_{\mathrm{II},\lambda_2}$ for two diamond-shaped holes at the corner A under three fundamental loads

		Uniaxial tension ($F_{\mathrm{I},\lambda_1} = K_{\mathrm{I},\lambda_1}/\sigma^\infty\sqrt{\pi}l^{1-\lambda_1}$, $F_{\mathrm{II},\lambda_2} = K_{\mathrm{II},\lambda_2}/\sigma^\infty\sqrt{\pi}l^{1-\lambda_2}$)						Biaxial tension ($F_{\mathrm{I},\lambda_1} = K_{\mathrm{I},\lambda_1}/\sigma^\infty\sqrt{\pi}l^{1-\lambda_1}$, $F_{\mathrm{II},\lambda_2} = K_{\mathrm{II},\lambda_2}/\sigma^\infty\sqrt{\pi}l^{1-\lambda_2}$)						In-plane shear ($F_{\mathrm{I},\lambda_1} = K_{\mathrm{I},\lambda_1}/\tau^\infty\sqrt{\pi}l^{1-\lambda_1}$, $F_{\mathrm{II},\lambda_2} = K_{\mathrm{II},\lambda_2}/\sigma^\infty\sqrt{\pi}l^{1-\lambda_2}$)					
		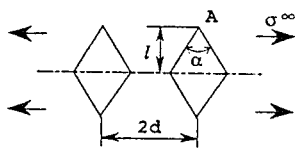						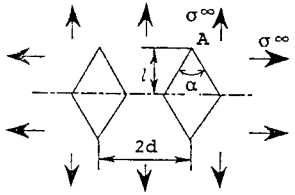						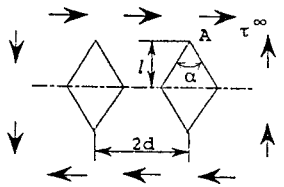					
l/d	α	0°	15°	20°	30°	60°	90°	0°	15°	20°	30°	60°	90°	0°	15°	20°	30°	60°	90°
0	F_{I,λ_1}	1.000	1.011	1.019	1.042	1.148	1.293	1.000	1.004	1.007	1.014	1.034	1.010	0.000	0.000	0.000	0.000	0.000	0.000
	$F_{\mathrm{II},\lambda_2}$	0.000	0.000	0.000	0.000	0.000	0.000	0.000	0.000	0.000	0.000	0.000	0.000	1.000	1.056	1.085	1.154	1.599	4.279
1/6	F_{I,λ_1}	0.990	1.001	1.009	1.029	1.133	1.275	0.990	0.994	0.997	1.004	1.024	1.002	0.001	0.001	0.001	0.001	0.002	0.003
	$F_{\mathrm{II},\lambda_2}$	0.001	0.001	0.001	0.001	0.003	0.010	0.001	0.001	0.001	0.001	0.002	0.004	1.003	1.063	1.090	1.160	1.608	4.312
1/4	F_{I,λ_1}	0.978	0.988	0.996	1.016	1.116	1.254	0.978	0.982	0.985	0.992	1.013	0.993	0.003	0.003	0.003	0.003	0.005	0.011
	$F_{\mathrm{II},\lambda_2}$	0.003	0.003	0.004	0.004	0.008	0.031	0.003	0.003	0.003	0.004	0.006	0.013	1.007	1.067	1.094	1.165	1.618	4.348
1/3	F_{I,λ_1}	0.964	0.973	0.980	0.999	1.096	1.228	0.964	0.968	0.971	0.977	0.998	0.982	0.006	0.007	0.007	0.008	0.012	0.026
	$F_{\mathrm{II},\lambda_2}$	0.006	0.007	0.008	0.009	0.018	0.067	0.006	0.007	0.007	0.008	0.012	0.028	1.012	1.072	1.100	1.171	1.629	4.390
1/2	F_{I,λ_1}	0.930	0.937	0.943	0.960	1.049	1.172	0.930	0.934	0.937	0.944	0.966	0.955	0.018	0.020	0.021	0.023	0.038	0.083
	$F_{\mathrm{II},\lambda_2}$	0.016	0.020	0.022	0.026	0.049	0.177	0.016	0.019	0.020	0.022	0.033	0.076	1.022	1.083	1.111	1.184	1.650	4.455
2/3	F_{I,λ_1}	0.895	0.901	0.907	0.923	1.006	1.125	0.895	0.901	0.904	0.911	0.935	0.923	0.038	0.041	0.043	0.048	0.080	0.188
	$F_{\mathrm{II},\lambda_2}$	0.031	0.038	0.041	0.048	0.088	0.305	0.031	0.036	0.038	0.042	0.061	0.152	1.030	1.092	1.121	1.194	1.662	4.436

Table 6. F_{I,λ_1} and $F_{\mathrm{II},\lambda_2}$ for two diamond-shaped holes at the corners B and B' under three fundamental loads

		Uniaxial tension: F_{I,λ_1} ($F_{\mathrm{I},\lambda_1} = K_{\mathrm{I},\lambda_1}/\sigma^{\infty}\sqrt{\pi}l^{1-\lambda_1}$)						Biaxial tension: F_{I,λ_1} ($F_{\mathrm{I},\lambda_1} = K_{\mathrm{I},\lambda_1}/\sigma^{\infty}\sqrt{\pi}l^{1-\lambda_1}$),)						In-plane shear: $F_{\mathrm{II},\lambda 2}$ ($F_{\mathrm{II},\lambda_2} = K_{\mathrm{II},\lambda_2}/\tau^{\infty}\sqrt{\pi}l^{1-\lambda_2}$)					
		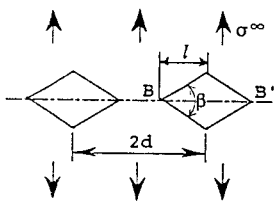						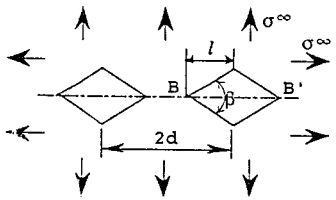						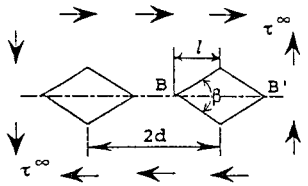					
l/d \ β		0°	15°	20°	30°	60°	90°	0°	15°	20°	30°	60°	90°	0°	15°	20°	30°	60°	90°
0	B, B'	1.000	1.011	1.019	1.042	1.148	1.293	1.000	1.004	1.007	1.014	1.034	1.010	1.000	1.056	1.085	1.154	1.599	4.279
1/6	B	1.004	1.022	1.027	1.048	1.152	1.295	1.004	1.014	1.015	1.021	1.041	1.020	1.004	1.065	1.092	1.161	1.611	4.323
	B'	1.003	1.021	1.026	1.047	1.152	1.295	1.003	1.014	1.014	1.021	1.040	1.018	1.003	1.064	1.091	1.160	1.608	4.306
1/4	B	1.009	1.024	1.032	1.053	1.157	1.296	1.009	1.016	1.020	1.027	1.047	1.033	1.009	1.069	1.099	1.169	1.626	4.392
	B'	1.007	1.023	1.028	1.051	1.155	1.297	1.007	1.016	1.016	1.025	1.044	1.027	1.007	1.068	1.096	1.165	1.616	4.333
1/3	B	1.018	1.030	1.041	1.062	1.164	1.299	1.018	1.023	1.029	1.036	1.057	1.052	1.018	1.078	1.109	1.181	1.650	4.507
	B'	1.012	1.025	1.036	1.057	1.160	1.300	1.012	1.018	1.024	1.031	1.051	1.038	1.012	1.072	1.102	1.172	1.626	4.365
1/2	B	1.048	1.064	1.072	1.092	1.190	1.317	1.048	1.057	1.060	1.067	1.093	1.111	1.048	1.117	1.148	1.226	1.743	4.944
	B'	1.028	1.042	1.052	1.072	1.174	1.313	1.028	1.035	1.040	1.046	1.069	1.065	1.028	1.089	1.119	1.191	1.654	4.434
2/3	B	1.112	1.130	1.137	1.156	1.252	1.374	1.112	1.123	1.126	1.133	1.168	1.210	1.112	1.195	1.231	1.325	1.949	5.888
	B'	1.052	1.069	1.076	1.096	1.197	1.338	1.052	1.062	1.064	1.071	1.097	1.101	1.052	1.117	1.145	1.218	1.689	4.504

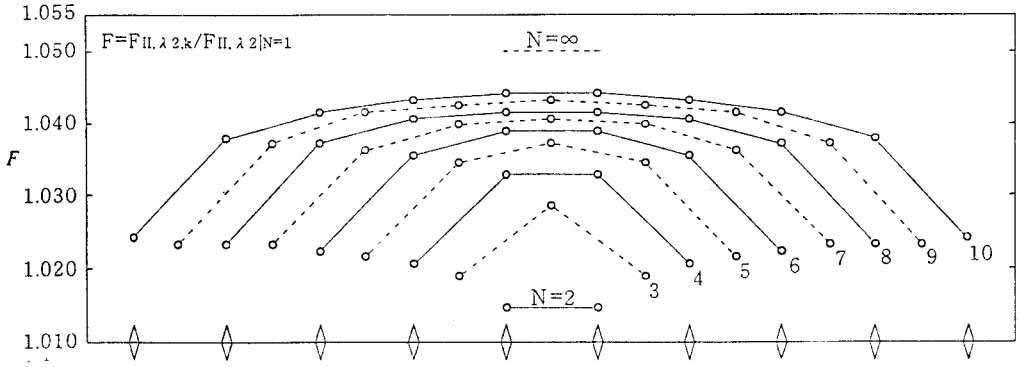

Figure 9. F for each diamond-shaped hole at the corner A. ($\tau_{xy}^{\infty} = \tau^{\infty}, \sigma_x^{\infty} = \sigma_y^{\infty} = 0$, $\alpha = 30°$, $\lambda = \frac{1}{3}$).

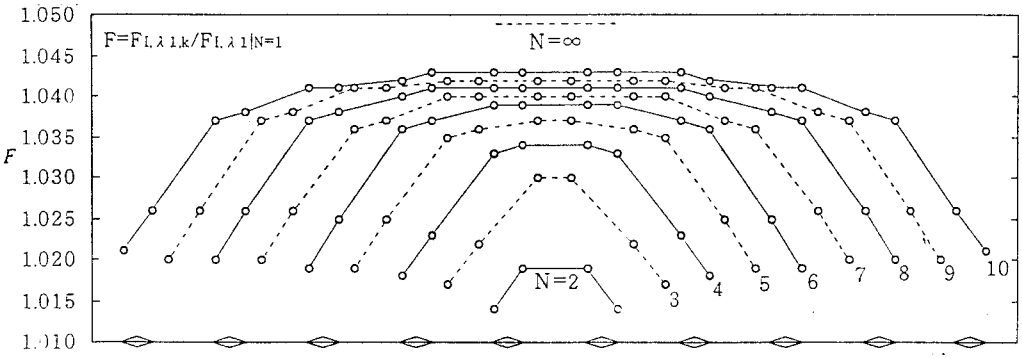

Figure 10. F for each diamond-shaped hole at the corners B and B'. ($\sigma_y^{\infty} = \sigma^{\infty}, \sigma_x^{\infty} = \tau_{xy}^{\infty} = 0$, $\beta = 30°$, $\lambda = \frac{1}{3}$).

the maximum stress intensity factors $F_{\max,N}$ ($F_{\mathrm{I}\max,N}$ or $F_{\mathrm{II}\max,N}$) occur at the outermost diamond-shaped holes. In Figures 9–11, $F_{\max,N}$ appears at the middle holes. From results under three types of loads, when $\alpha \leqslant 90°$, $F_{\mathrm{I}\max,N}$ occurs at the outermost diamond-shaped holes under uniaxial and biaxial tension and $F_{\mathrm{II}\max,N}$ occurs at the middle holes under in-plane shear. On the other hand, when $\beta \leqslant 90°$, $F_{\max,N}$ occurs at the middle holes under three types of loads. Those results are similar to the problems of parallel and collinear cracks [16].

Tables 7 and 8 show the values of the maximum stress intensity factors $F_{\max,N}$ ($F_{\mathrm{I}\max,N}$ or $F_{\mathrm{II}\max,N}$) when the values of N, $\lambda = l/d$ and α (or β) are changed systematically. Figures 12–14 show $F_{\mathrm{I}\max,N} - 1/N$ relations when $\sigma_y^{\infty} = \sigma^{\infty}, \sigma_x^{\infty} = \tau_{xy}^{\infty} = 0, \lambda = \frac{1}{3}, \frac{1}{2}, \frac{2}{3}$. From these figures, the stress intensity factors are found to be nearly linear with $1/N$ for fixed values of λ. In these tables and figures, the limiting values for $N \to \infty$ are extrapolated from the values for $N = 9$ and $N = 10$ by using the linearity between $F_{\max,N}$ and $1/N$. As shown in Tables 7, 8 and Figures 12–14, the interaction effect of diamond-shaped holes appears in a similar way to the results of collinear and parallel ordinary cracks [16].

4. Conclusions

In this paper, numerical solution of singular integral equations was discussed in the analysis of angular corners. The extended stress intensity factors of the problem were calculated very

Table 7. $F_{\max,N}$ for any diamond−shaped holes at the corner A under three fundamental loads

	λ	$\alpha = 0^\circ$					$\alpha = 30^\circ$					$\alpha = 60^\circ$					$\alpha = 90^\circ$				
		$F\|_{N=1}$	$F_{\max,N}/F\|_{N=1}$				$F\|_{N=1}$	$F_{\max,N}/F\|_{N=1}$				$F\|_{N=1}$	$F_{\max,N}/F\|_{N=1}$				$F\|_{N=1}$	$F_{\max,N}/F\|_{N=1}$			
N		0	0	$\frac{1}{3}$	$\frac{1}{2}$	$\frac{2}{3}$	0	0	$\frac{1}{3}$	$\frac{1}{2}$	$\frac{2}{3}$	0	0	$\frac{1}{3}$	$\frac{1}{2}$	$\frac{2}{3}$	0	0	$\frac{1}{3}$	$\frac{1}{2}$	$\frac{2}{3}$
Uniaxial tension	2	1.000	1.000	0.964	0.930	0.896	1.042	1.000	0.958	0.921	0.886	1.148	1.000	0.954	0.914	0.876	1.293	1.000	0.949	0.907	0.870
$(F\|_{N=1} = F_{\mathrm{I},\lambda_1}, F_{\max,N} = F_{\mathrm{I}\max,N})$	3	1.000	1.000	0.955	0.915	0.876	1.042	1.000	0.951	0.907	0.867	1.148	1.000	0.945	0.898	0.856	1.293	1.000	0.939	0.890	0.849
	4	1.000	1.000	0.952	0.909	0.867	1.042	1.000	0.947	0.900	0.857	1.148	1.000	0.941	0.891	0.847	1.293	1.000	0.934	0.882	0.840
	5	1.000	1.000	0.949	0.905	0.862	1.042	1.000	0.944	0.896	0.852	1.148	1.000	0.938	0.887	0.842	1.293	1.000	0.931	0.878	0.834
	6	1.000	1.000	0.948	0.902	0.859	1.042	1.000	0.943	0.894	0.849	1.148	1.000	0.936	0.884	0.838	1.293	1.000	0.930	0.875	0.831
	7	1.000	1.000	0.947	0.901	0.856	1.042	1.000	0.942	0.892	0.846	1.148	1.000	0.935	0.882	0.836	1.293	1.000	0.929	0.873	0.828
	8	1.000	1.000	0.947	0.900	0.855	1.042	1.000	0.941	0.891	0.844	1.148	1.000	0.935	0.881	0.834	1.293	1.000	0.928	0.871	0.826
	9	1.000	1.000	0.946	0.899	0.854	1.042	1.000	0.941	0.890	0.843	1.148	1.000	0.934	0.880	0.832	1.293	1.000	0.927	0.870	0.825
	10	1.000	1.000	0.946	0.898	0.853	1.042	1.000	0.940	0.889	0.842	1.148	1.000	0.933	0.879	0.831	1.293	1.000	0.926	0.869	0.823
	∞	1.000	1.000	0.942	0.892	0.846	1.042	1.000	0.936	0.881	0.832	1.148	1.000	0.929	0.871	0.821	1.293	1.000	0.922	0.861	0.813
Biaxial tension	2	1.000	1.000	0.964	0.930	0.896	1.014	1.000	0.964	0.931	0.898	1.034	1.000	0.966	0.934	0.904	1.010	1.000	0.972	0.945	0.914
$(F\|_{N=1} = F_{\mathrm{I},\lambda_1}, F_{\max,N} = F_{\mathrm{I}\max,N})$	3	1.000	1.000	0.955	0.915	0.876	1.014	1.000	0.956	0.917	0.881	1.034	1.000	0.959	0.923	0.890	1.010	1.000	0.967	0.938	0.908
	4	1.000	1.000	0.952	0.909	0.867	1.014	1.000	0.953	0.911	0.872	1.034	1.000	0.955	0.917	0.883	1.010	1.000	0.965	0.935	0.906
	5	1.000	1.000	0.949	0.905	0.862	1.014	1.000	0.951	0.908	0.868	1.034	1.000	0.954	0.914	0.879	1.010	1.000	0.963	0.933	0.904
	6	1.000	1.000	0.948	0.902	0.859	1.014	1.000	0.949	0.905	0.865	1.043	1.000	0.952	0.912	0.877	1.010	1.000	0.962	0.932	0.903
	7	1.000	1.000	0.947	0.901	0.856	1.014	1.000	0.948	0.904	0.863	1.034	1.000	0.951	0.911	0.875	1.010	1.000	0.962	0.931	0.902
	8	1.000	1.000	0.947	0.900	0.855	1.014	1.000	0.948	0.903	0.861	1.034	1.000	0.951	0.910	0.874	1.010	1.000	0.961	0.930	0.902
	9	1.000	1.000	0.946	0.899	0.854	1.014	1.000	0.947	0.902	0.860	1.034	1.000	0.950	0.909	0.873	1.010	1.000	0.961	0.930	0.902
	10	1.000	1.000	0.946	0.898	0.853	1.014	1.000	0.947	0.901	0.859	1.034	1.000	0.950	0.909	0.872	1.010	1.000	0.961	0.930	0.901
	∞	1.000	1.000	0.942	0.892	0.846	1.014	1.000	0.943	0.894	0.850	1.034	1.000	0.947	0.903	0.864	1.010	1.000	0.958	0.926	0.898
In-plane shear	2	1.000	1.000	1.012	1.022	1.030	1.154	1.000	1.014	1.026	1.034	1.599	1.000	1.018	1.032	1.039	4.279	1.000	1.026	1.041	1.037
$(F\|_{N=1} = F_{\mathrm{II},\lambda_2}, F_{\max,N} = F_{\mathrm{II}\max,N})$	3	1.000	1.000	1.024	1.044	1.059	1.154	1.000	1.029	1.052	1.070	1.599	1.000	1.036	1.064	1.081	4.279	1.000	1.052	1.084	1.076
	4	1.000	1.000	1.028	1.051	1.073	1.154	1.000	1.033	1.061	1.086	1.599	1.000	1.042	1.077	1.103	4.279	1.000	1.061	1.105	1.112
	5	1.000	1.000	1.031	1.059	1.087	1.154	1.000	1.037	1.070	1.102	1.599	1.000	1.048	1.089	1.124	4.279	1.000	1.070	1.125	1.149
	6	1.000	1.000	1.033	1.063	1.094	1.154	1.000	1.039	1.075	1.110	1.599	1.000	1.050	1.096	1.137	4.279	1.000	1.074	1.136	1.170
	7	1.000	1.000	1.034	1.067	1.101	1.154	1.000	1.041	1.080	1.119	1.599	1.000	1.053	1.102	1.149	4.279	1.000	1.078	1.147	1.192
	8	1.000	1.000	1.035	1.069	1.105	1.154	1.000	1.042	1.082	1.124	1.599	1.000	1.054	1.106	1.156	4.279	1.000	1.081	1.154	1.207
	9	1.000	1.000	1.036	1.072	1.110	1.154	1.000	1.043	1.085	1.129	1.599	1.000	1.056	1.110	1.164	4.279	1.000	1.083	1.161	1.221
	10	1.000	1.000	1.037	1.073	1.112	1.154	1.000	1.044	1.087	1.132	1.599	1.000	1.057	1.112	1.169	4.279	1.000	1.085	1.165	1.231
	∞	1.000	1.000	1.043	1.088	1.142	1.154	1.000	1.050	1.103	1.164	1.599	1.000	1.066	1.135	1.214	4.279	1.000	1.099	1.205	1.336

Table 8. $F_{\max,N}$ for any diamond–shaped holes at the corner B and B' under three fundamental loads

	λ	$\beta = 0^\circ$					$\beta = 30^\circ$					$\beta = 60^\circ$					$\beta = 90^\circ$				
		$F\|_{N=1}$	$F_{\max,N}/F\|_{N=1}$				$F\|_{N=1}$	$F_{\max,N}/F\|_{N=1}$				$F\|_{N=1}$	$F_{\max,N}/F\|_{N=1}$				$F\|_{N=1}$	$F_{\max,N}/F\|_{N=1}$			
N		0	0	$\frac{1}{3}$	$\frac{1}{2}$	$\frac{2}{3}$	0	0	$\frac{1}{3}$	$\frac{1}{2}$	$\frac{2}{3}$	0	0	$\frac{1}{3}$	$\frac{1}{2}$	$\frac{2}{3}$	0	0	$\frac{1}{3}$	$\frac{1}{2}$	$\frac{2}{3}$
Uniaxial tension	2	1.000	1.000	1.018	1.048	1.115	1.042	1.000	1.019	1.048	1.110	1.148	1.000	1.014	1.037	1.090	1.293	1.000	1.006	1.018	1.063
$(F\|_{N=1} = F_{\mathrm{I},\lambda_1}, F_{\max,N} = F_{\mathrm{I}\max,N})$	3	1.000	1.000	1.031	1.077	1.172	1.042	1.000	1.030	1.074	1.161	1.148	1.000	1.023	1.059	1.136	1.293	1.000	1.010	1.035	1.102
	4	1.000	1.000	1.035	1.088	1.199	1.042	1.000	1.034	1.085	1.187	1.148	1.000	1.026	1.068	1.159	1.293	1.000	1.012	1.042	1.124
	5	1.000	1.000	1.039	1.097	1.218	1.042	1.000	1.037	1.093	1.204	1.148	1.000	1.029	1.075	1.174	1.293	1.000	1.014	1.048	1.139
	6	1.000	1.000	1.041	1.102	1.230	1.042	1.000	1.039	1.098	1.216	1.148	1.000	1.030	1.079	1.184	1.293	1.000	1.015	1.052	1.149
	7	1.000	1.000	1.043	1.106	1.240	1.042	1.000	1.040	1.102	1.224	1.148	1.000	1.031	1.082	1.192	1.293	1.000	1.015	1.055	1.156
	8	1.000	1.000	1.044	1.108	1.246	1.042	1.000	1.041	1.104	1.230	1.148	1.000	1.032	1.085	1.198	1.293	1.000	1.016	1.056	1.161
	9	1.000	1.000	1.044	1.111	1.251	1.042	1.000	1.042	1.106	1.235	1.148	1.000	1.033	1.087	1.202	1.293	1.000	1.016	1.058	1.166
	10	1.000	1.000	1.045	1.112	1.255	1.042	1.000	1.043	1.108	1.239	1.148	1.000	1.033	1.088	1.206	1.293	1.000	1.017	1.059	1.169
	∞	1.000	1.000	1.052	1.128	1.293	1.042	1.000	1.049	1.123	1.275	1.148	1.000	1.038	1.101	1.238	1.293	1.000	1.020	1.071	1.201
Biaxial tension	2	1.000	1.000	1.018	1.048	1.115	1.014	1.000	1.022	1.052	1.117	1.034	1.000	1.022	1.057	1.129	1.010	1.000	1.041	1.100	1.198
$(F\|_{N=1} = F_{\mathrm{I},\lambda_1}, F_{\max,N} = F_{\mathrm{I}\max,N})$	3	1.000	1.000	1.031	1.077	1.172	1.014	1.000	1.032	1.079	1.171	1.034	1.000	1.037	1.090	1.192	1.010	1.000	1.068	1.154	1.291
	4	1.000	1.000	1.035	1.088	1.199	1.014	1.000	1.037	1.091	1.199	1.034	1.000	1.042	1.103	1.222	1.010	1.000	1.076	1.174	1.333
	5	1.000	1.000	1.039	1.097	1.218	1.014	1.000	1.040	1.100	1.217	1.034	1.000	1.046	1.113	1.243	1.010	1.000	1.084	1.189	1.362
	6	1.000	1.000	1.041	1.102	1.230	1.014	1.000	1.042	1.105	1.229	1.034	1.000	1.048	1.119	1.256	1.010	1.000	1.087	1.198	1.376
	7	1.000	1.000	1.043	1.106	1.240	1.014	1.000	1.044	1.109	1.238	1.034	1.000	1.050	1.124	1.266	1.010	1.000	1.090	1.205	1.395
	8	1.000	1.000	1.044	1.108	1.246	1.014	1.000	1.045	1.111	1.245	1.034	1.000	1.051	1.127	1.274	1.010	1.000	1.093	1.210	1.405
	9	1.000	1.000	1.044	1.111	1.251	1.014	1.000	1.045	1.114	1.250	1.034	1.000	1.052	1.129	1.280	1.010	1.000	1.094	1.214	1.414
	10	1.000	1.000	1.045	1.112	1.255	1.014	1.000	1.046	1.115	1.254	1.034	1.000	1.053	1.131	1.284	1.010	1.000	1.096	1.217	1.420
	∞	1.000	1.000	1.052	1.128	1.293	1.014	1.000	1.052	1.132	1.292	1.034	1.000	1.060	1.150	1.327	1.010	1.000	1.108	1.245	1.480
In-plane shear	2	1.000	1.000	1.018	1.048	1.115	1.154	1.000	1.023	1.063	1.148	1.599	1.000	1.032	1.090	1.219	4.279	1.000	1.053	1.155	1.376
$(F\|_{N=1} = F_{\mathrm{II},\lambda_2}, F_{\max,N} = F_{\mathrm{II}\max,N})$	3	1.000	1.000	1.031	1.077	1.172	1.154	1.000	1.037	1.094	1.207	1.599	1.000	1.049	1.125	1.284	4.279	1.000	1.074	1.197	1.459
	4	1.000	1.000	1.035	1.088	1.199	1.154	1.000	1.042	1.108	1.242	1.599	1.000	1.056	1.146	1.336	4.279	1.000	1.087	1.234	1.539
	5	1.000	1.000	1.039	1.097	1.218	1.154	1.000	1.046	1.118	1.264	1.599	1.000	1.061	1.159	1.364	4.279	1.000	1.094	1.253	1.582
	6	1.000	1.000	1.041	1.102	1.230	1.154	1.000	1.049	1.124	1.279	1.599	1.000	1.064	1.168	1.388	4.279	1.000	1.100	1.269	1.625
	7	1.000	1.000	1.043	1.106	1.240	1.154	1.000	1.051	1.129	1.290	1.599	1.000	1.067	1.175	1.403	4.279	1.000	1.104	1.279	1.651
	8	1.000	1.000	1.044	1.108	1.246	1.154	1.000	1.052	1.133	1.299	1.599	1.000	1.068	1.180	1.416	4.279	1.000	1.107	1.289	1.676
	9	1.000	1.000	1.044	1.111	1.251	1.154	1.000	1.053	1.135	1.305	1.599	1.000	1.070	1.184	1.426	4.279	1.000	1.109	1.295	1.6[illegible]
	10	1.000	1.000	1.045	1.112	1.255	1.154	1.000	1.054	1.138	1.311	1.599	1.000	1.071	1.187	1.434	4.279	1.000	1.111	1.301	1.71[illegible]
	∞	1.000	1.000	1.052	1.128	1.293	1.154	1.000	1.061	1.157	1.359	1.599	1.000	1.081	1.215	1.511	4.279	1.000	1.127	1.354	1.869

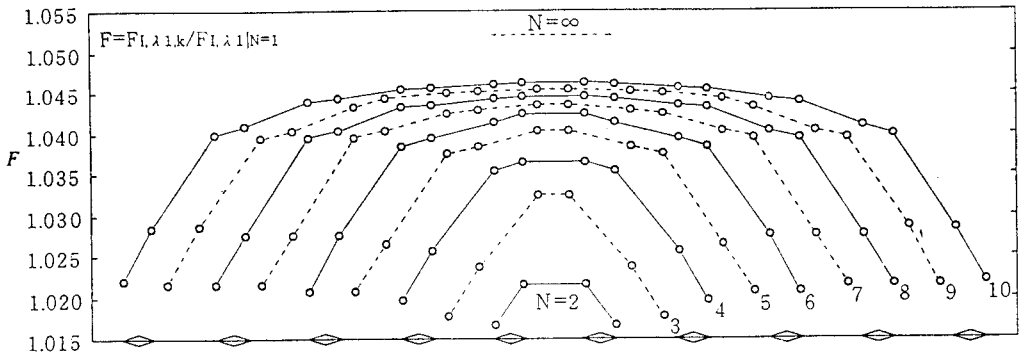

Figure 11. F for each diamond-shaped hole at the corners B and B'. ($\sigma_x^\infty = \sigma_y^\infty = \sigma^\infty, \tau_{xy}^\infty = 0$, $\beta = 30°$, $\lambda = \frac{1}{3}$).

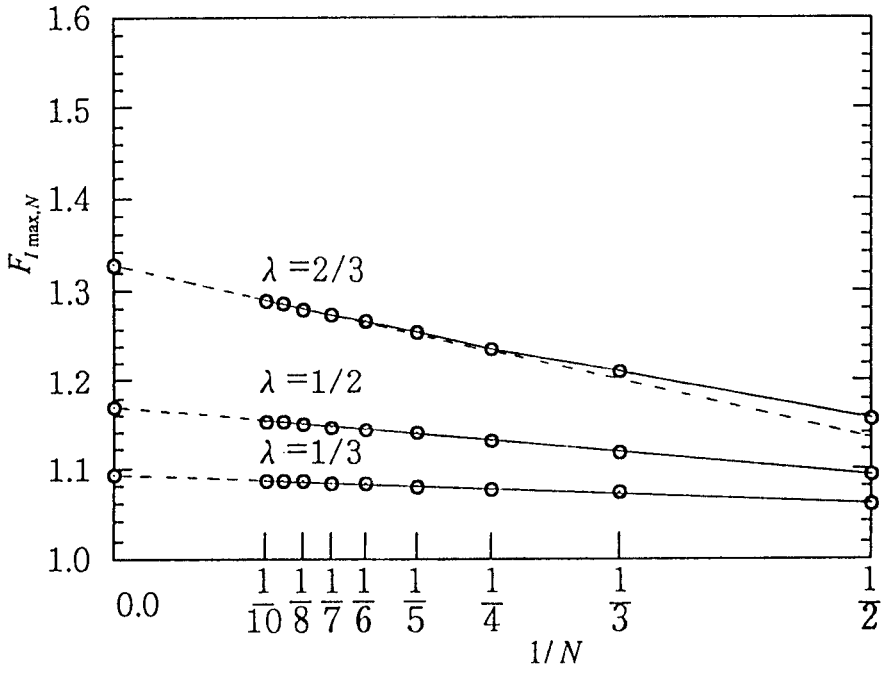

Figure 12. $F_{I\,max,N} - 1/N$ relations. ($\sigma_y^\infty = \sigma^\infty, \sigma_x^\infty = \tau_{xy}^\infty = 0$, $\beta = 30°$).

accurately by using the singular integral equations of the body force method. The interaction effect of angular corners was also considered under various geometries and loadings. The conclusions can be made as follows.

(1) The problems of the angular corner were formulated as a system of singular integral equations of the body force method. In this problem the unknown functions were approximated by using power series and two types of fundamental density functions, that is, symmetric type (mode I) and skew-symmetric type (mode II). The calculation showed that the method gave the rapidly converging numerical results and two types of stress intensity factors K_{I,λ_1}, K_{II,λ_2} were obtained with high accuracy.

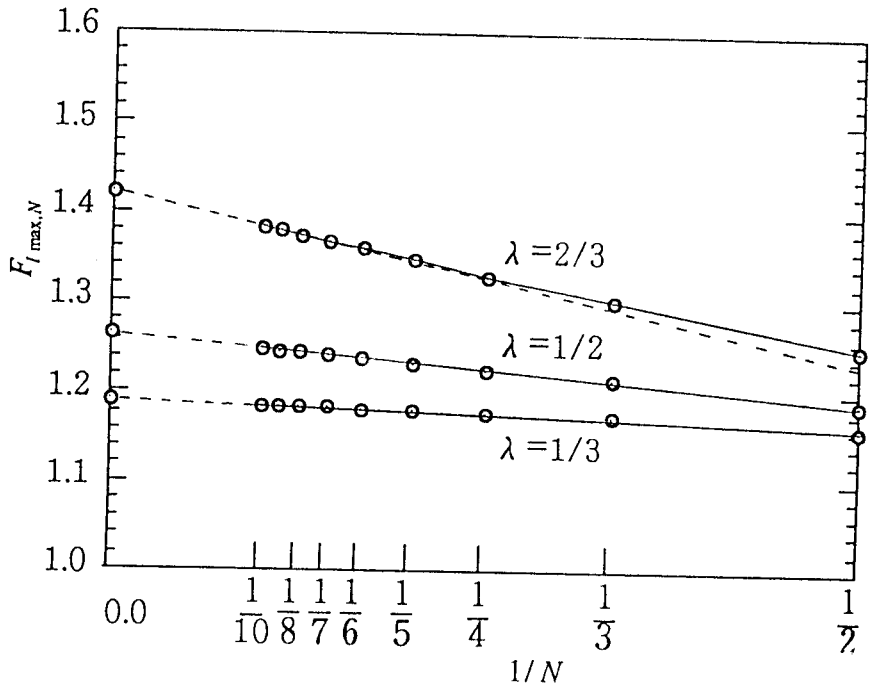

Figure 13. $F_{I\max,N} - 1/N$ relations. ($\sigma_y^\infty = \sigma^\infty, \sigma_x^\infty = \tau_{xy}^\infty = 0,\ \beta = 60°$).

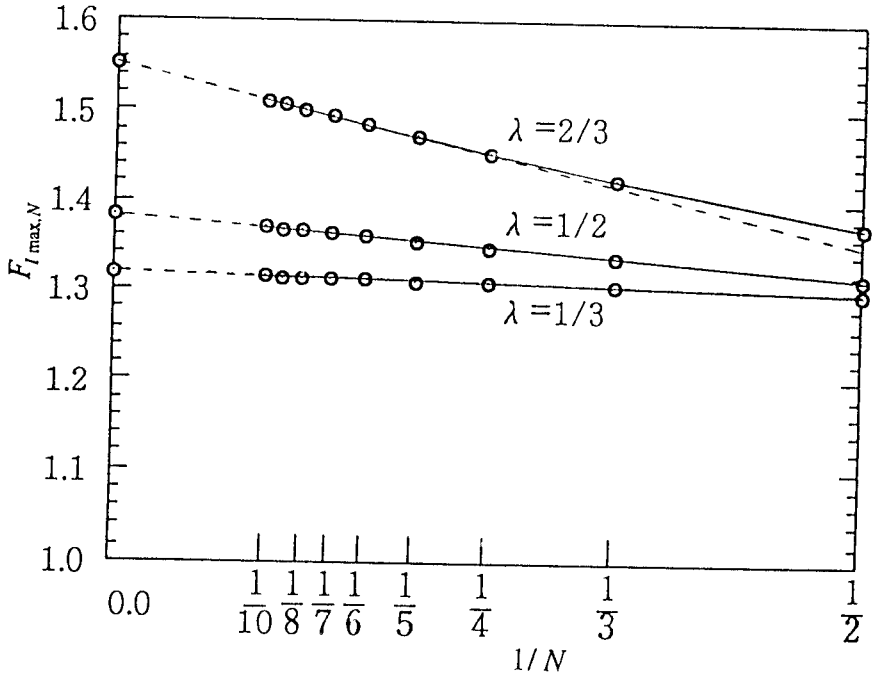

Figure 14. $F_{I\max,N} - 1/N$ relations. ($\sigma_y^\infty = \sigma^\infty, \sigma_x^\infty = \tau_{xy}^\infty = 0,\ \beta = 90°$).

(2) A parallelogram hole in an infinite plate (Figure 3) and a V-shaped notch in a semi-infinite plate (Figure 4) were analyzed as fundamental problems of an angular corner. The results of the V-shaped notch in a semi-infinite plate were in good agreement with the results obtained by Chen and Nisitani. The relation between the dimensionless SIFs of the angular corner and the inclination angle γ was similar to that of cracks. Namely, F_{I,λ_1}-values for a semi-infinite plate were always larger than those for an infinite plate in all the ranges of $0° \leqslant \gamma \leqslant 45°$. On the other hand, $F_{\mathrm{II},\lambda_2}$-values for a semi-infinite plate were always smaller than those for an infinite plate.

(3) The interaction problems of two and any number of diamond-shaped holes with the same shape and size under various loading conditions were analyzed (Figure 1). When $\alpha \leqslant 90°$, $F_{\mathrm{I}\max,N}$ occurred at the outermost diamond-shaped holes under uniaxial and biaxial tension. On the other hand, under in-plane shear, $F_{\mathrm{II}\max,N}$ occurred at the middle diamond-shaped holes. Those results were similar to the interaction effect of the parallel cracks.

(4) When $\beta \leqslant 90°$, $F_{\max,N}$ ($F_{\mathrm{I}\max,N}$ or $F_{\mathrm{II}\max,N}$) occurred at the middle diamond-shaped holes under all three types of loads. These results were similar to the interaction effect of the collinear cracks.

(5) The stress intensity factors of angular corners were found to be nearly linear with $1/N$ (N: number of holes) for fixed values of λ. Based on this information, $F_{\max,N}$ for any number of N could be estimated.

References

1. M.L. Williams, *Transactions of the ASME, Journal of Applied Mechanics* 19 (1952) 526–528.
2. J.P. Dempsey and G.B. Sinclair, *Journal of Elasticity* 9 (1979) 373–391.
3. *Ibid.*, 11 (1981) 317–327.
4. D.B. Bogy, *Transactions of the ASME, Journal of Applied Mechanics* 35 (1968) 460–466.
5. *Ibid.*, 38 (1971) 377–386.
6. D.B. Bogy and K.C. Wang, *International Journal of Solids and Structures* 7 (1971) 993–1005.
7. V.L. Heim and F. Erdogan, *International Journal of Fracture Mechanics* 7 (1971) 317–330.
8. P.S. Theocaris, *International Journal of Engineering Science* 12 (1974) 107–120.
9. D.H. Chen and H. Nisitani, *Transactions of the Japan Society of Mechanical Engineers* 57-534 A (1991) 366–372.
10. *Ibid.*, 57-538 A (1991) 1406–1411.
11. D.H. Chen and H. Nisitani, *Transactions of the ASME, Journal of Applied Mechanics* 60 (1993) 607–613.
12. N.-A. Noda, H. Umeki and F. Erdogan, *Transactions of the Japan Society of Mechanical Engineers* 55-520 A (1989) 2521–2526.
13. N.-A. Node and K. Oda, *International Journal of Fracture* 58 (1992) 285–304.
14. *Ibid.*, 64 (1993) 239–249.
15. F. Erdogan, *Proceedings 4th U.S. National Congress for Applied Mechanics* (1962) 547–553.
16. M. Isida and H. Igawa, *Transactions of the Japan Society of Mechanical Engineers* 59-561 A (1993) 1263–1269.
17. H. Nisitani, *Journal of the Japan Society of Mechanical Engineers* 70 (1967) 627–632. [*Bulletin of Japan Society of Mechanical Engineers* 11 (1968) 14–23.]
18. H. Nisitani, *Mechanics of Fracture 5, Stress Analysis of Notched Problem*, G.C. Sih (ed.), Leyden (1978) 1–68.